Acta Montanistica Slovaca
ISSN 1335-1788
actamont.tuke.sk

Changes in the structure of red mud and black nickel mud after activation

Maroš SOLDÁN[1], Tomáš ŠTEFKO[2], Igor WACHTER[1], Renata NAVICKIENĖ[2] and Hana KOBETIČOVÁ[1]*

Authors' affiliations and addresses:
[1] Slovak University of Technology in Bratislava, Faculty of Materials Science and Technology in Trnava, Slovakia
e-mail: maros.soldan@stuba.sk

[2] Institute of Sustainable Development
Aušros av. 66 A
76233 Šiauliai
Lithuania
e-mail: info@institute.lt

***Correspondence:**
Maroš Soldán, Slovak University of Technology in Bratislava, Faculty of Materials Science and Technology in Trnava, Slovakia
tel.: 0918 646 066
e-mail: maros.soldan@stuba.sk

Funding information:
Slovak Research and Development Agency contract No. APVV-21-0187
KEGA Agency contract No. KEGA 016STU-4/2021
VEGA agency contract No. VEGA 1/0678/22

How to cite this article:
Soldán, M., Štefko, T., Wachter, I., Navickienė, R. and Kobetičová, H. (2024). Changes in the structure of red mud and black nickel mud after activation. *Acta Monstanistica Slovaca*, Volume 29 (1), 227-236

DOI:
https://doi.org/10.46544/AMS.v29i1.20

Abstract
This paper deals with the evaluation of the structure of selected hazardous wastes from the production of metals, namely waste from the production of aluminium - red mud and waste from the production of nickel - black nickel mud. In environmental applications, red mud and black nickel mud are likely to be used after activation. The samples were activated using hydrochloric acid to study the structure properties before and after the treatment. Both of these wastes have suitable adsorption and catalytic properties that could be positively affected by the activation of their surfaces. The morphology of the samples was documented by scanning electron microscope, phase analysis was performed using diffraction techniques, and the content of elements was determined by EDX analysis. Also, FTIR analysis of the samples was performed. Activation increases the specific surface area of samples, which is beneficial in many environmental applications, such as in the adsorptive removal of pollutants. Treatment of samples changes the surface properties of the adsorbent, such as electrostatic, hydrophobic, and hydrophilic. The activation creates a new surface structure and thus affects its properties. EDX analysis confirmed the high content of Fe, Al, Si and Ti, which are responsible for good adsorption and catalytic properties. X-ray diffractograms have shown only slight changes in the structure of wastes after activation. The results of SEM confirmed the changes in the surface structure and the creation of new active centres necessary for the successful adsorption process. The FTIR analysis determined the changes in the structure of the samples mainly due to the thermal degradation of C=O and O-Si-O bonds.

Keywords
Black nickel mud; EDX analysis; Electron microscopy; FTIR spectrometry; Red mud; X-ray analysis

Introduction

The manufacturing of alumina from refined bauxite produces bauxite residue, also known as red mud (RM), a type of strong alkaline solid waste. Due to its high production and significant alkalinity, RM poses significant environmental risks (Liu *et al.*, 2023). For every ton of alumina produced, 1.0 to 1.8 tons of RM are produced on average, with approximately 140 million metric tonnes of alumina produced worldwide in 2022 (U.S. Geological Survey, 2023). The Bayer process is now the primary method used to produce alumina, as more than 90% of the world's total alumina production is manufactured using it (Gou *et al.*, 2023). The rate of alumina production at the refinery and the quantity of 'available' alumina in the bauxite are the two main factors affecting the amount generated by RM. A minor, though essential, effect is the refinery processing conditions and the kind of alumina minerals present (such as gibbsite, boehmite, or diaspore). More than 4 billion tonnes of RM has been generated worldwide, with an annual growth rate of approximately 150 million of tonnes (International Aluminium Institute, 2022). Only 8% of the total amount of RM produced is reused.

There are numerous issues related to RM storage. Many alumina smelters employ landfills, pond or marine disposal, and dry pile-up as their primary means of RM disposal. These techniques demand a lot of storage space, containment systems, and additional costs (Kang and Kim, 2023). In addition, RM has a high pH (10−13) and some heavy metals due to the caustic soda used in Bayer's process. When RM's wastewater containing solid alkaline leaks into the ground during wet storage, the groundwater is contaminated, the nearby soil becomes alkaline, and crop growth is hampered (Qaidi *et al.*, 2022a).

Additionally, when exposed to the air for an extended period of time, the deposited RM will turn into dust, seriously harming the environment (Winkler *et al.*, 2018). The vast bulk of generated RM is held in "Bauxite Residue Storage Facilities" (BRSFs), as just a fraction of it exits the residue regions of refineries. The methods used for processing and storing bauxite leftovers are influenced by a number of variables, including the refinery's age, the availability of land, its closeness to the sea, the geography of the area, the climate, logistics, the type of the residue, and laws (International Aluminium Institute, 2022).

While RM storage can mitigate environmental harm momentarily, it cannot fundamentally address the issue of environmental pollution (Feng *et al.*, 2020). There are many studies on various applications of RM, but very few have been successfully commercialized. The majority investigated the utilization of RM is technically possible but not commercially viable. A few uses are commercially viable but will not significantly reduce the vast amounts of RM generated each year (International Aluminium Institute, 2022).

The range of applications currently in use or under development utilise RM:

- as a bulk material, with or without additions and/or simple treatments (e.g. covering landfill (Ujaczki *et al.*, 2016) and soil (Berta *et al.*, 2021), land remediation (Wang and Liu, 2021), road and pavement base (Zhang *et al.*, 2021), cement addition (Patangia *et al.*, 2023));
- as a secondary source of the other minerals and metals components (value extraction) (e.g. iron (Kong *et al.*, 2022), titanium (Shoppert and Loginova, 2017), rare earths (Agrawal and Dhawan, 2021)(Samal, 2021));
- as a construction material (by processing), (e.g. bricks (Zhang *et al.*, 2023; Dodok *et al.*, 2017), tiles (Wang *et al.*, 2018), geopolymers and pigments (Elhag *et al.*, 2023; Kopas *et al.* 2017));
- for a specialised property or application by using more advanced processing (e.g. aggregates (Qian *et al.*, 2023), proppants (Tian, Wu and Li, 2008), water treatment reagents (Wang and Liu, 2021), catalysts (Chen, Wang and Liu, 2023)).

The utilisation of RM will benefit the environment and the economy by reducing landfill volume (Blistan *et al.*, 2020; Kovanič *et al.*, 2021), removing soil and groundwater pollution, and freeing up space for other applications. It may also be used to manufacture valuable materials for other uses, therefore preserving natural resources.

Many efforts have been undertaken in recent years to utilise RM components in bulk applications, notably in water treatment. RM has the potential to be used in water treatment for the removal of hazardous heavy metal and metalloid ions, organic pollutants such as bacteria, dyes, and phenolic compounds, and inorganic anions such as nitrate, fluoride, and phosphate (Wang, Ang and Tadé, 2008). The RM has a specific surface area of roughly 12-59 $m^2 g^{-1}$, a grain width of 0.005 to 0.075 mm, and a porosity ratio that is much greater than that of typical soil (Khairul, Zanganeh and Moghtaderi, 2019)(Wang *et al.*, 2021)(Wang *et al.*, 2019). As a result, RM has excellent adsorption properties and is well-suited for usage as a heavy metal adsorbent (Qaidi *et al.*, 2022b).

RM poses, under certain circumstances, a potential hazard even though it is generally considered normal solid waste. For example, according to U.S. EPA (U.S. Environmental Protection Agency) or Chinese Identification standards for hazardous wastes (GB5085.3-2007), it is not included in the list of hazardous wastes (Liu *et al.*, 2021). Hazardous properties of RM, such as flammability, reactivity, and infectiousness, are much lower than for conventional hazardous wastes. As a result, the two key criteria for evaluating RM's

environmental impacts are its toxicity and corrosivity. The presence of heavy metal components may also be used to determine the radioactivity threat of RM (Pérez-Villarejo *et al.*, 2012).

The black nickel mud (BNM) is a byproduct of the nickel and cobalt-based processing. In this paper, a BNM from imported Albanian ferro-nickel lateritic ore with a nickel concentration of 1% per ton was studied. The annual output of BNM was around 300,000 kg, with supply in Slovakia estimated at 5.6 million tons. It comprises chromium oxide, silicon aluminium, and calcium, with the remainder primarily being iron concentrate. This waste's high chromium concentration and roughness limit its usage in metallurgy. Due to the low chromium content, using this waste to manufacture ferrochrome is not viable. The removal of it as an ingredient to cement by the building materials sector was halted due to the appearance aspect of chromium, which is not permitted as an additive under European regulations (Kovacova *et al.*, 2009)(Václaviková *et al.*, 2002).

The main findings described in the article concern the evaluation of the structure of RM from the landfill in Slovakia (residue from Hungarian bauxite) and BNM (residue from Albanian nickel ore). The structure and chemical composition were evaluated before and after chemical activation. The described activation process could have positive effects on the adsorption and catalytic properties of both wastes. The structure of RM is described thoroughly in the scientific literature, but this type of RM is not. The structure of black nickel mud has not yet been evaluated. Due to its structure and chemical composition identified in this study, it could be more effective in adsorption or catalysis than RM.

Materials and Methods

Samples of RM and BNM were activated by chemical procedure:

10 g of sample was pretreated with 18 ml of 31 % HCl with the addition of 190 ml of distilled water, heated for 20 minutes at 100 °C and subsequently filled with distilled water up to 800 ml. Adjustment of the pH to the desired value (pH=8) was performed using a 22% NH_3 solution. Suspension was heated for 10 minutes to 50 °C, filtered and three times decanted with distilled water. The sample was dried at 110 °C and annealed at 550 °C for 2 hours (Chen, Wang and Liu, 2023; Pivarciova et al., 2019).

The JEOL JSM 7600 F high-resolution scanning electron microscope (SEM) with a FEG cathode equipped with EDX (Energy - dispersion X-ray. detector) the detector was used for sample analysis. Oxinst MAX 50. The samples were scanned in a special mode, environmental SEM (ESEM), which uses extremely low voltage acceleration (0.1 to 3 kV). In this mode, accelerated electrons are slowed down by a negative bias just before impacting the sample to reduce the electron's kinetic energy and increase the rate of electrons emitting from the sample. The charging of the sample by the electric charge, which is carried by the electron, is also significantly reduced.

Fourier transform infrared spectrometry (FTIR) was used to analyze the samples of RM and BNM using the Varian 660 MidIRDual MCT / DTGS Bundle. A highly sensitive FTIR spectrometer was used in the dual arrangement of MCT / DTGS detectors with a diamond ATR GladiATR in the 400-4000 cm-1 range. Spectrum was measured 100 times with a resolution of 4 cm^{-1}, a filter of 1.28 kHz and a rate of 5 kHz, recorded and evaluated using VarianResolutionsPro software with the Sadtler Canadian Forensics library.

Results

According to the EDX analysis, the most abundant elements in RM samples are Ca, Fe, Al, Si, O, and Ti, followed by an array of minor constituents, including Cl, Mn, and Cr. These results confirmed a higher percentage of Fe and Al, which can positively affect waste's adsorption and catalytic properties. Acid treatment and calcination of RM samples have changed the physicochemical properties that affect the catalytic activity. After activation of the surface of RM, the reduction of Ca and Mg occurred, which is caused by a reaction of calcium ions with HCl (Tab. 1).

Tab. 1 Composition of red mud sample by EDX analysis (wt%).

	O	Al	Si	Mg	Ca	Fe	Cl	Ti	Mn
Nonactivated RM	36.46	4.79	3.53	2.51	3.60	41.45	0.16	3.03	0.44
Activated RM	36.95	4.29	6.60	0.13	0.99	46.22	0.13	3.26	0.29

A similar phenomenon was observed in BNM, where the concentration of Mg after activation was reduced similarly (Tab. 2). The zero nickel content in the sample was due to its complete extraction from the original ore.

Tab. 2 Composition of black nickel mud sample by EDX analysis (wt%).

	O	Al	Si	Mg	Ca	Fe	Cl	Ti	Mn
Nonactivated BNM	33.75	2.42	3.53	1.34	3.15	49.95	0.10	1.67	0.61
Activated BNM	26.17	3.62	6.60	1.30	1.10	56.39	0.23	1.99	0.68

We have found no significant changes in X-ray diffractograms of activated and nonactivated forms of RM. The samples consist mainly of hematite (Fe_2O_3), calcium, and titanium-containing perovskite ($CaTiO_3$) and rutile (TiO_2). We have also identified cancrinite katoite ($Ca_3Al_{3\cdot5}O_{4\cdot5}(OH)_{7.5}$), gibbsite ($Al(OH)_3$), ($Na_7Ca_{0\cdot9}Al_6(SiO_4)_6(CO_3)_{1\cdot4}(H_2O)_{2.1}$), calcium, and titanium containing perovskite ($CaTiO_3$) and calcium carbonate ($CaCO_3$). During the acid activation (removal of elements) and calcination (oxidation of hydroxides) of RM, cancrinite, katoite, and gibbsite were converted. Inactivated RM and aluminium compounds are considered to be amorphous. (Fig. 1, Fig. 2).

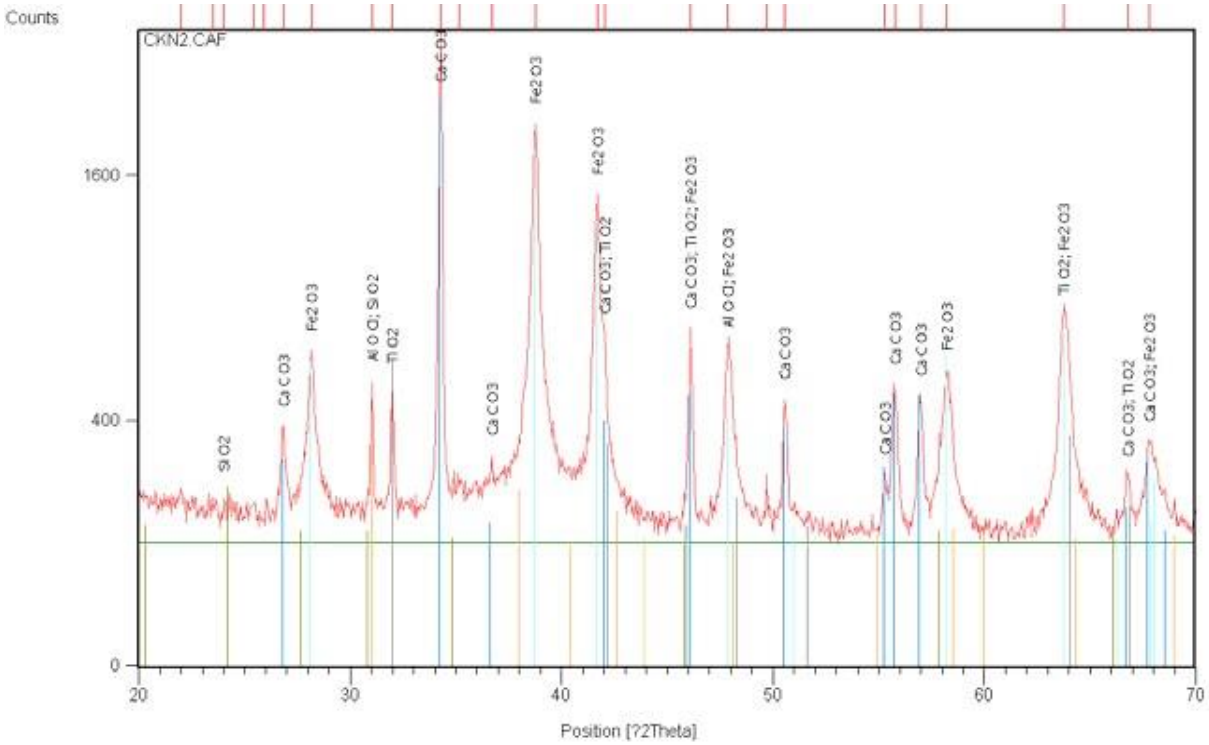

Fig. 1 RTG diffractogram of nonactivated red mud.

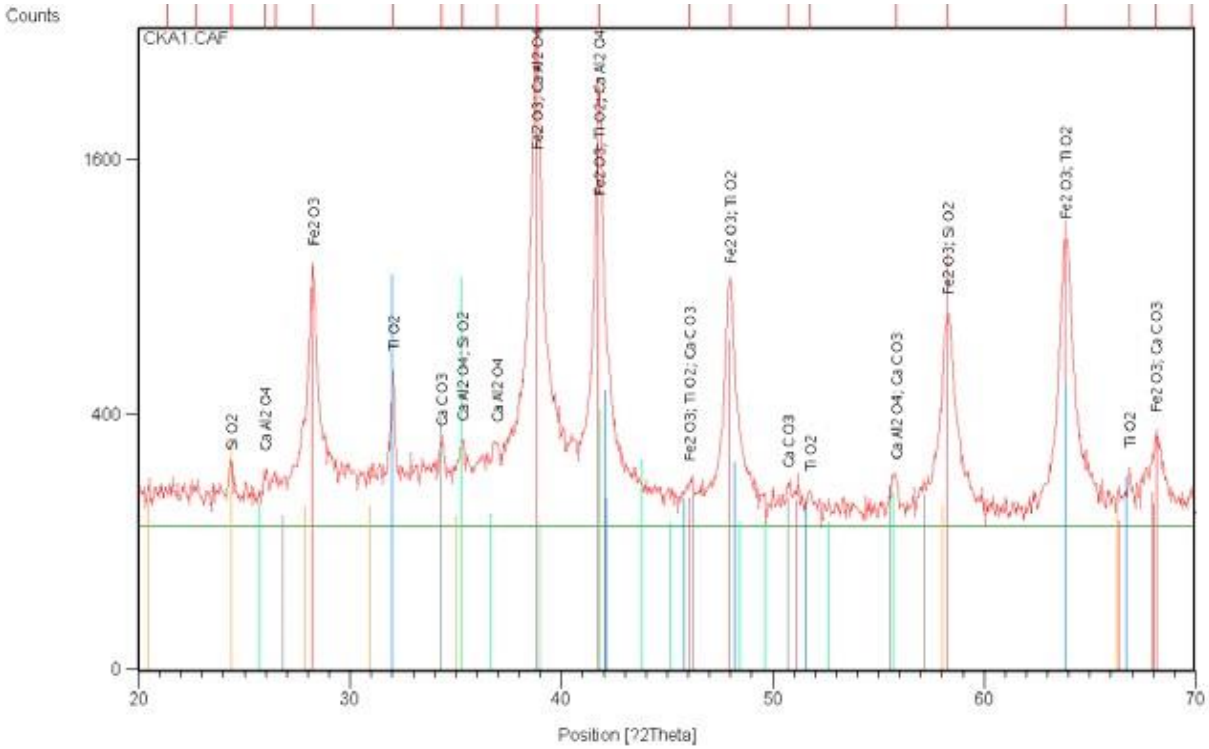

Fig. 2 . RTG diffractogram of activated red mud.

Hematite, schorlomite $Ca_3(Fe, Ti)[(Si, Ti)O]$, calcite ($CaCO_3$), magnetite (FeO), and sillimanite (AlSiO) (Fig. 3, Fig. 4) are presented in the samples of BNM. The concentration of $CaCO_3$ and schorlomite was significantly decreased by surface activation of the BNM. After activation, the iron concentration of crystalline compounds reduces, most likely as a result of heat treatment. The detection of specific metal oxides validated the usage of chosen wastes as adsorbents or catalysts.

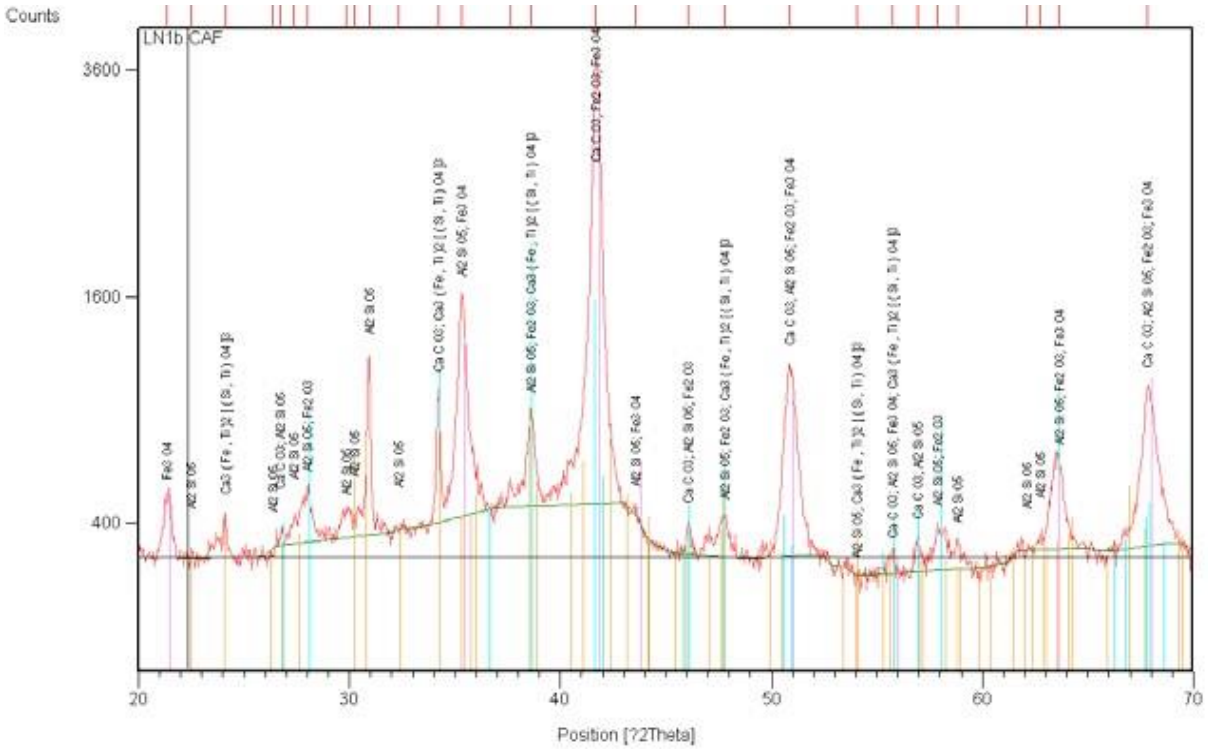

Fig. 3 RTG diffractogram of nonactivated black nickel mud.

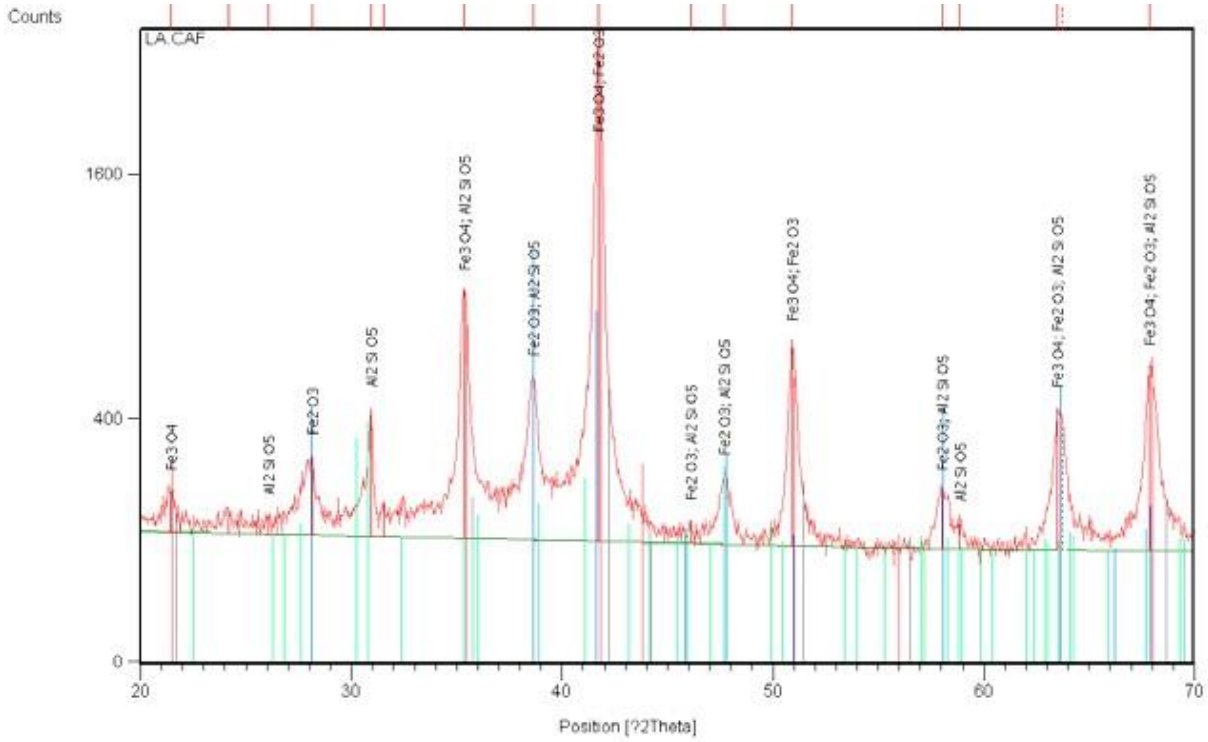

Fig. 4 RTG diffractogram of activated black nickel mud.

The shape of RM and BNM was studied using scanning electron microscopy (SEM). Microscopically, RM is composed of microscopic granules ranging in size from millimetres to microns. The irregular morphologies of

RM, which include flaky and spherical granules, characterize it. Most of the time, agglomeration produces enormous aggregates of much smaller particles. Particles are found to be amorphous materials that are crystalline, widely scattered, and even disorderly. Because of particle agglomeration, there are gaps between tiny particles. The surface area of RM is greater after activation. New cavities and granular structures are present in the acid-activated samples, which have an effect on their properties. The large specific surface area and porous structure of RM could improve its adsorption capabilities while also influencing its interfacial adhesion behaviour. The surface of nonactivated RM is relatively rough in morphology. The size of the particles varies from 0.5 to 1 μm. The changes in the smooth surface porous structure were observed after chemical activation. Dissolution of surface salts in the presence of acid led to the creation of crystalline structures (Fig. 5).

The morphological difference of BNM samples was observed when compared to RM samples. Surface layers of particles of BNM also formed agglomerates of nickel mud, which retain their original form. The change of the specific surface area after activation was less significant than in RM. The activation of the surface of BNM significantly caused the fragmentation of particles, which ultimately increased the specific surface area mainly due to a reduction in particle diameter (Fig. 6).

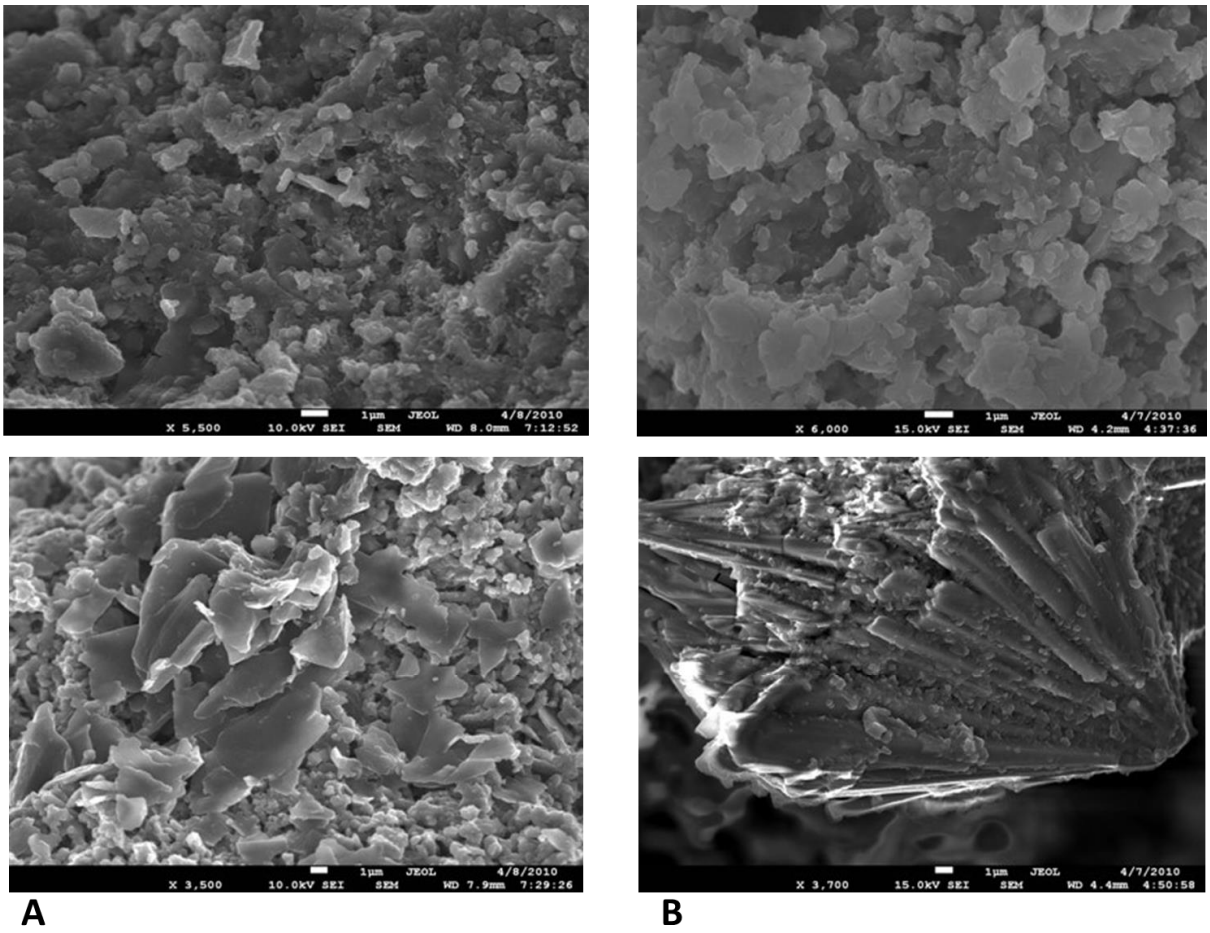

Fig. 5 The surface of activated (A) and nonactivated (B) red mud.

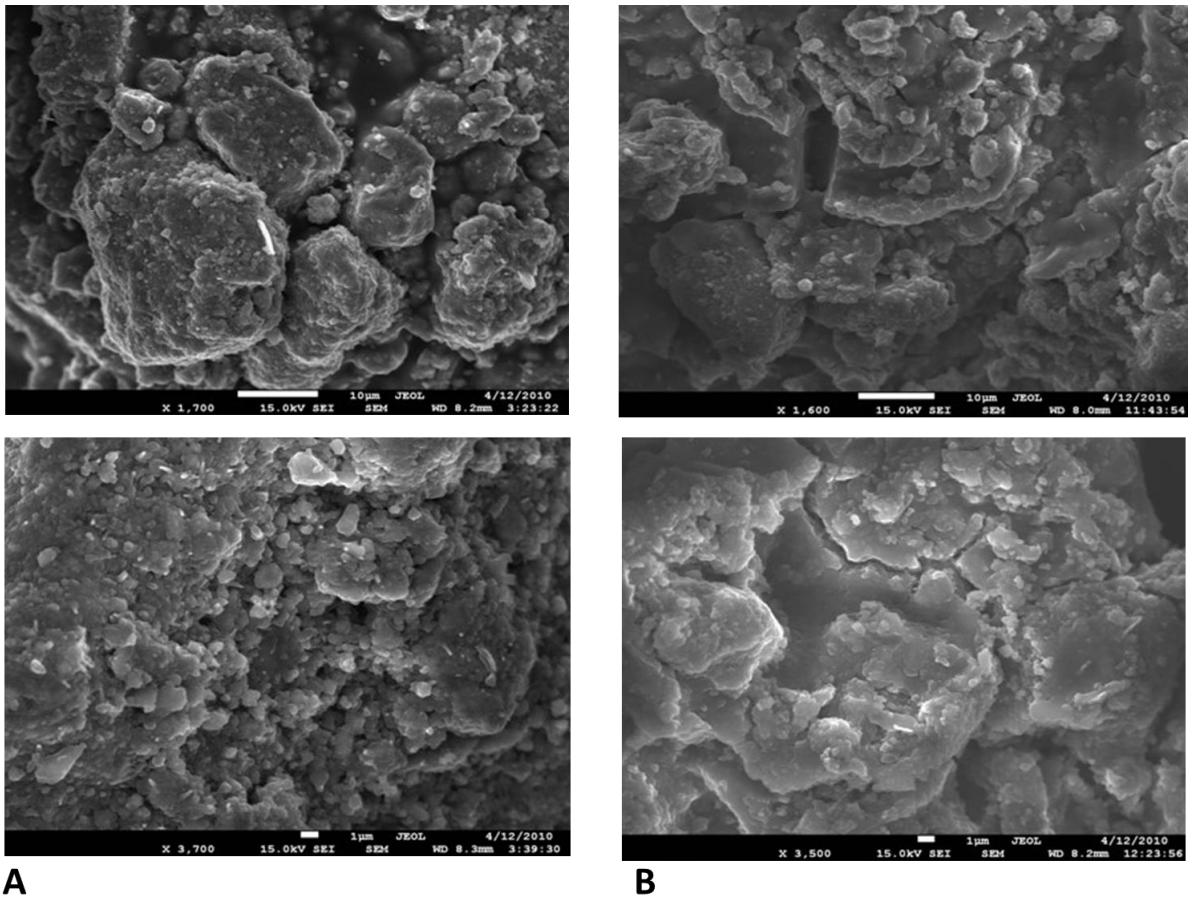

Fig. 6 The surface of activated (A) and nonactivated (B) black nickel mud.

FTIR spectrum of RM samples before and after activation is shown in Fig. 7. An intensive absorption band can be observed in the wavelength range of 1440 cm^{-1}, which can be classified as the stretching vibration of the C = O bond. The primary reason for observing these bonds is the presence of chemically-sorbed CO_2 on the RM surface. After activation, the intensity of the C=O bond decreases because CO_2 is released from the surface. The important absorption band at 990 cm^{-1} corresponds to the vibration of Si-O. Its intensity decreases after activation mainly due to the thermal degradation of the mineral compounds. The small adsorption peak at 870 cm^{-1} belongs to the Al-O bond. The adsorption band at 530 cm^{-1} corresponds to the vibrations of the O-Si-O groups. The absorption peak, observed at 450 $cm^{-1,}$ is characteristic of the vibration of the Fe-O bond. In the 3600 – 3400 cm-1 region, the identified absorbent band is associated with vibrations of O-H and / H-O-H bonds of adsorbed water molecules. After activation, these bonds disappear due to the evaporation of moisture during annealing (Pechac *et al.*, 2016).

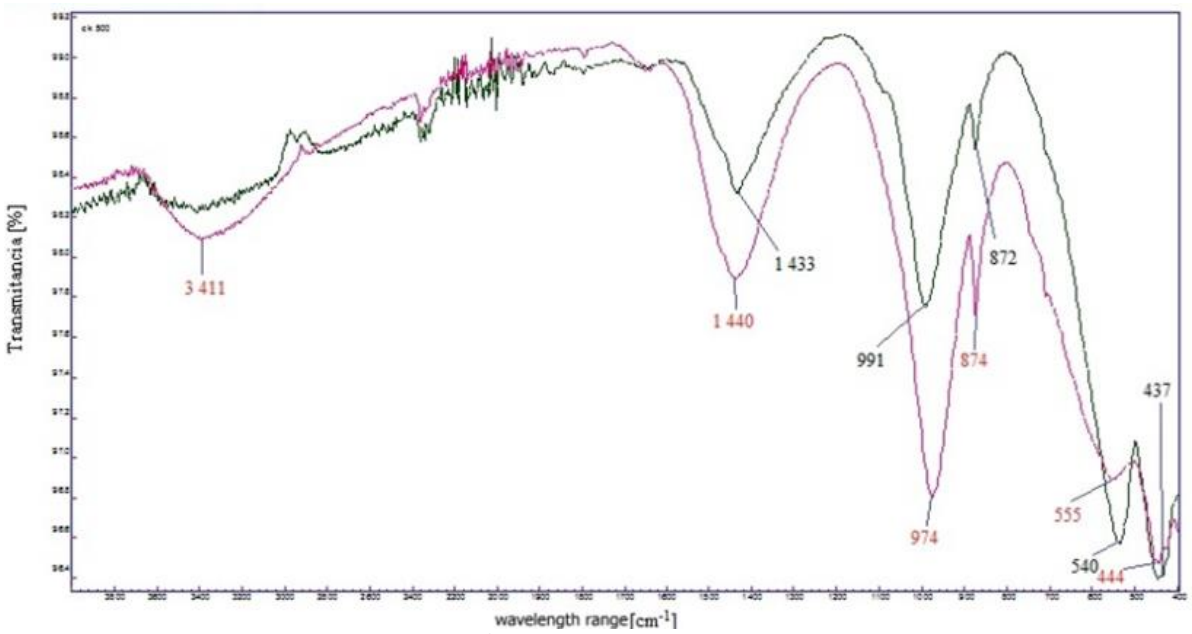

Fig. 7 The FTIR spectra of nonactivated (red line) and activated (green line) RM.

FTIR spectra of the BNM are shown in Figure 8. In the wavelength range 530 $cm^{-1,}$ we can observe a non-distinctive band corresponding to the vibrations of the O–Si–O groups. The intensity did not change after the activation. Al-O bonds are typical for a smaller adsorption peak in the wavelength range of 870 cm^{-1}. After activation, these bonds degrade, resulting in a decrease in the intensity of the peak. The absorption peak at 980 cm^{-1} corresponds to Si-O vibrations. In the wavelength range of 1 500 cm^{-1}, an intensive absorption band is observed corresponding to the O-H bonds in the water molecule. This band almost disappears in the sample of activated BNM.

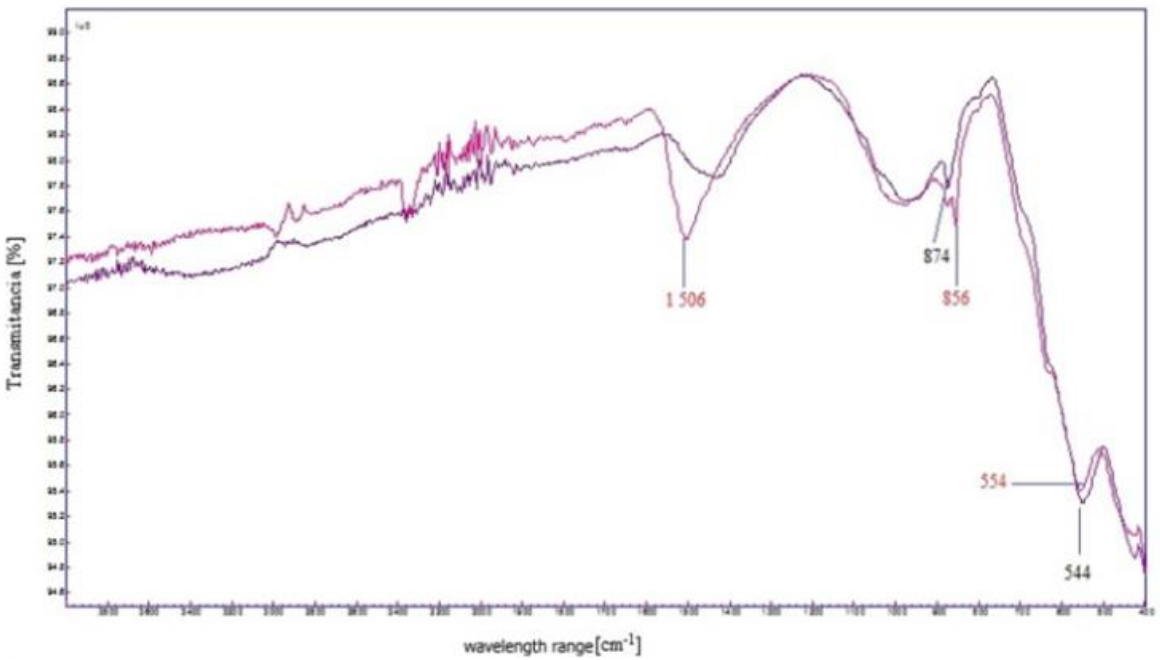

Fig. 8 The FTIR spectra of nonactivated (red line) and activated (green line) BNM.

Conclusions

The structure of RM and BNM before and after chemical activation was studied. Studying the X-ray diffractograms of activated and nonactivated forms of red mud and black nickel mud, it was found that activation of red mud led to a significant reduction in $CaCO_3$ content and activation of black nickel mud caused a significant decrease of $CaCO_3$ and schorlomite. EDX analysis of the samples confirmed the higher percentage

content of Fe and Al, which will positively affect the adsorption and catalytic properties. The results of SEM confirmed the changes in the porosity of the structure and the creation of new active centres. The FTIR analysis determined the changes in the structure of the samples that were caused by the thermal treatment.

It could be concluded that the activation positively affects the properties of selected wastes from the metal-producing industry. It has changed the surface properties, mainly electrostatic, hydrophobic, and hydrophilic. Changes in the particle structure of the surface were also determined. The presence of new cavities and roughened surface structure was observed mainly due to the dissolution of compounds on the surface using HCl. The activation creates a new surface structure and thus affects its properties. This could be used in sorption and catalytic processes to remove hazardous substances from water solutions. This was also supported by EDX and FTIR analysis. Both muds have been characterized, and potential applications for using them can be devised.

References

Agrawal, S. and Dhawan, N. (2021) 'Evaluation of red mud as a polymetallic source – A review', Minerals Engineering, 171, p. 107084. doi: https://doi.org/10.1016/j.mineng.2021.107084.

Berta, K. M. et al. (2021) 'Red mud with other waste materials as artificial soil substitute and its effect on Sinapis alba', Journal of Environmental Management, 287, p. 112311. doi: https://doi.org/10.1016/j.jenvman.2021.112311.

Blistan, P.; Jacko, S.; Kovanič, Ľ.; Kondela, J.; Pukanská, K.; Bartoš, K. TLS and SfM Approach for Bulk Density Determination of Excavated Heterogeneous Raw Materials. *Minerals* 2020, *10*, 174. https://doi.org/10.3390/min10020174

Chen, J., Wang, Y. and Liu, Z. (2023) 'Red mud-based catalysts for the catalytic removal of typical air pollutants: A review', Journal of Environmental Sciences, 127, pp. 628–640. doi: https://doi.org/10.1016/j.jes.2022.06.027.

Dodok, T., (2017) Workshop programming as a part of technological preparation of production. ADVANCES IN SCIENCE AND TECHNOLOGY-RESEARCH JOURNAL. Volume 11, Issue 1, Page 111-116. DOI10.12913/22998624/66504Elhag, A. B. et al. (2023) 'A critical review on mechanical, durability, and microstructural properties of industrial by-product-based geopolymer composites'. (REVIEWS ON ADVANCED MATERIALS SCIENCE), 62(1). doi: doi:10.1515/rams-2022-0306.

Feng, Y. et al. (2020) 'A Study of Strength Mechanism of Mixed Red Mud and the Influence of Acid', Environmental Engineering Science. Mary Ann Liebert, Inc., publishers, 37(4), pp. 272–282. doi: 10.1089/ees.2019.0277.

Gou, M. et al. (2023) 'Preparation and properties of calcium aluminate cement with Bayer red mud', Construction and Building Materials, 373, p. 130827. doi: https://doi.org/10.1016/j.conbuildmat.2023.130827. International Aluminium Institute (2022) Sustainable Bauxite Residue Management Guidance. London.

Kang, C. and Kim, T. (2023) 'Development of construction materials using red mud and brine', Case Studies in Construction Materials, 18, p. e02185. doi: https://doi.org/10.1016/j.cscm.2023.e02185.

Khairul, M. A., Zanganeh, J. and Moghtaderi, B. (2019) 'The composition, recycling and utilisation of Bayer red mud', Resources, Conservation and Recycling, 141, pp. 483–498. doi: https://doi.org/10.1016/j.resconrec.2018.11.006.

Kong, H. et al. (2022) 'Iron Recovery Technology of Red Mud—A review', Energies. doi: 10.3390/en15103830.

Kopas, P. et al. (2017) Identification of mechanical properties of weld joints of AlMgSi07.F25 aluminium alloy, Metalurgija, Volume 56, Issue1-2, Page 99-102.

Kovacova, M. et al. (2009) 'Microwave Vitrification of Model Heavy Metals Carriers From Wastewaters Treatment', MRS Online Proceedings Library, 1193(1), p. 323. doi: 10.1557/PROC-1193-323.

Kovanič, Ľ.; Blistan, P.; Štroner, M.; Urban, R.; Blistanova, M. Suitability of Aerial Photogrammetry for Dump Documentation and Volume Determination in Large Areas. *Appl. Sci.* 2021, *11*, 6564. https://doi.org/10.3390/app11146564

Liu, S. et al. (2023) 'The roles of red mud as desulfurization and denitrification in flue gas: A review', Journal of Environmental Chemical Engineering, 11(3), p. 109770. doi: https://doi.org/10.1016/j.jece.2023.109770.

Liu, X. et al. (2021) 'Characteristic, hazard and iron recovery technology of red mud - A critical review', Journal of Hazardous Materials, 420, p. 126542. doi: https://doi.org/10.1016/j.jhazmat.2021.126542.

Patangia, J. et al. (2023) 'Study on the utilization of red mud (bauxite waste) as a supplementary cementitious material: Pathway to attaining sustainable development goals', Construction and Building Materials, 375, p. 131005. doi: https://doi.org/10.1016/j.conbuildmat.2023.131005.

Pechac, P. et al. (2016) Controlling of local search methods' parameters in memetic algorithms using the principles of simulated annealing, 20 TH INTERNATIONAL CONFERENCE MACHINE MODELING AND SIMULATIONS, MMS 2015, Volume 136, Page 70-76, DOI10.1016/j.proeng.2016.01.176

Pérez-Villarejo, L. et al. (2012) 'Manufacturing new ceramic materials from clay and red mud derived from the aluminium industry', Construction and Building Materials, 35, pp. 656–665. doi: https://doi.org/10.1016/j.conbuildmat. 2012.04.133.

Pivarciova, E. et al. (2019) 'Design of the construction and research of vibrations and heat transfer of mine workings', Acta montanistica Slovavaca, Volume 24, Issue 1, Page 15-24.

Qaidi, S. M. A. et al. (2022a) 'RETRACTED: Sustainable utilization of red mud waste (bauxite residue) and slag for the production of geopolymer composites: A review', Case Studies in Construction Materials, 16, p. e00994. doi: https://doi.org/10.1016/j.cscm.2022.e00994.

Qaidi, S. M. A. et al. (2022b) 'Sustainable utilization of red mud waste (bauxite residue) and slag for the production of geopolymer composites: A review', Case Studies in Construction Materials, 16, p. e00994. doi: https://doi.org/10.1016/j.cscm.2022.e00994.

Qian, L.-P. et al. (2023) 'Recycling of red mud and flue gas residues in geopolymer aggregates (GPA) for sustainable concrete', Resources, Conservation and Recycling, 191, p. 106893. doi: https://doi.org/10.1016/j.resconrec.2023.106893.

Samal, S. (2021) 'Utilization of Red Mud as a Source for Metal Ions-A Review.', Materials (Basel, Switzerland). Switzerland, 14(9). doi: 10.3390/ma14092211.

Shoppert, A. and Loginova, I. (2017) 'Red Mud as an Additional Source of Titanium Raw Materials', KnE Materials Science, 2, p. 150. doi: 10.18502/kms.v2i2.962.

Tian, X., Wu, B. and Li, J. (2008) 'The exploration of making acidproof fracturing proppants using red mud', Journal of Hazardous Materials, 160(2), pp. 589–593. doi: https://doi.org/10.1016/j.jhazmat.2008.03.032.

U.S. Geological Survey (2023) Mineral commodity summaries 2023, Mineral Commodity Summaries. Reston, VA. doi: 10.3133/mcs2023.

Ujaczki, É. et al. (2016) 'The potential application of red mud and soil mixture as additive to the surface layer of a landfill cover system', Journal of Environmental Sciences, 44, pp. 189–196. doi: https://doi.org/10.1016/j.jes.2015.12.014.

Václaviková, M. et al. (2002) ‘Odstraňovanie iónov Pb2+, Cd2+ a Co2+ z vôd pomocou magnetických sorbentov’, Acta Montanistica Slovaca, 7(1), pp. 23–27.

Wang, L. et al. (2019) 'A Review on Comprehensive Utilization of Red Mud and Prospect Analysis', Minerals. doi: 10.3390/min9060362.

Wang, M. and Liu, X. (2021) 'Applications of red mud as an environmental remediation material: A review', Journal of Hazardous Materials, 408, p. 124420. doi: https://doi.org/10.1016/j.jhazmat.2020.124420.

Wang, S. et al. (2021) 'Comprehensive utilization status of red mud in China: A critical review', Journal of Cleaner Production, 289, p. 125136. doi: https://doi.org/10.1016/j.jclepro.2020.125136.

Wang, S., Ang, H. M. and Tadé, M. O. (2008) 'Novel applications of red mud as coagulant, adsorbent and catalyst for environmentally benign processes', Chemosphere, 72(11), pp. 1621–1635. doi: https://doi.org/10.1016/j.chemosphere.2008.05.013.

Wang, W. et al. (2018) 'Recycling of waste red mud for production of ceramic floor tile with high strength and lightweight', Journal of Alloys and Compounds, 748, pp. 876–881. doi: https://doi.org/10.1016/j.jallcom.2018.03.220.

Winkler, D. et al. (2018) 'Long-term ecological effects of the red mud disaster in Hungary: Regeneration of red mud flooded areas in a contaminated industrial region', Science of The Total Environment, 644, pp. 1292–1303. doi: https://doi.org/10.1016/j.scitotenv.2018.07.059.

Zhang, J. et al. (2021) 'Sustainable utilization of bauxite residue (Red Mud) as a road material in pavements: A critical review', Construction and Building Materials, 270, p. 121419. doi: https://doi.org/10.1016/j.conbuildmat.2020.121419.

Zhang, J. et al. (2023) 'Preparation of building ceramic bricks using waste residue obtained by mutual treatment of electrolytic manganese residue and red mud', Ceramics International, 49(13), pp. 22492–22505. doi: https://doi.org/10.1016/j.ceramint.2023.04.083.